Computational Investigation of Adsorption of Molecular Hydrogen on Lithium-Doped Corannulene

Y. Zhang,[†] L. G. Scanlon,[‡] M. A. Rottmayer,[‡] and P. B. Balbuena*,[†]

Department of Chemical Engineering, Texas A&M University, College Station, Texas 77843, and Air Force Research Laboratory, Energy Storage & Thermal Sciences Branch, Wright−Patterson Air Force Base, Ohio 45433

Received: June 24, 2006; In Final Form: August 14, 2006

Density functional theory and classical molecular dynamics simulations are used to investigate the prospect of lithium-doped corannulene as adsorbent material for H_2 gas. Potential energy surface scans at the level of B3LYP/6-311G(d,p) show an enhanced interaction of molecular hydrogen with lithium-atom-doped corannulene complexes with respect to that found in undoped corannulene. MP2(FC)/6-31G(d,p) optimizations of $4H_2-(Li_2-C_{20}H_{10})$ yield H_2 binding energies of −1.48 kcal/mol for the H_2-Li interaction and −0.92 kcal/mol for the H_2-C interaction, whereas values of −0.94 and −0.83 kcal/mol were reported (*J. Phys. Chem. B* **2006**, *110*, 7688−7694) for physisorption of H_2 on the concave and the convex side of corannulene using MP2-(full)/6-31G(d), respectively. Classical molecular dynamics simulations predict hydrogen uptakes in Li-doped corannulene assemblies that are significantly enhanced with respect to that found in undoped molecules, and the hydrogen uptake ability is dependent on the concentration of lithium dopant. For the $Li_6-C_{20}H_{10}$ complex, a hydrogen uptake of 4.58 wt % at 300 K and 230 bar is obtained when the adsorbent molecules are arranged in stack configurations separated by 6.5 Å, and with interlayer distances of 10 Å, hydrogen uptake reaches 6.5 wt % at 300 K and 215 bar.

1. Introduction

Hydrogen has been proposed as a potential clean fuel,[1] but in order to be commercially employed, it is critical to develop compact, low-cost, and safe storage materials. The U.S. Department of Energy (DOE) set up the criteria of storing 6.5 wt % of hydrogen (density of 62.5 Kg/m^3) for an ideal energy hydrogen carrier. Other than storage in high-pressure tanks as gas or cryogenic hydrogen, different advanced hydrogen storage materials have been extensively studied, including metal hydrides (MHs),[2−5] carbon-based,[6−13] and organometallic materials.[14−19]

The main mechanism of hydrogen adsorption on metal hydrides is chemisorption, and thus the desorption of hydrogen occurs at temperatures above 500 K and/or the hydrogen uptake capacity is low, about 2 wt %, due to the presence of heavy metals.[2−5] Hydrogen adsorption in carbon-based and organometallic materials is caused by physisorption. Organometallic materials[14−19] possess a low density, high surface area, and are porous materials. Hydrogen adsorption on organometallic materials shows about 4.5 wt % at 77 K and 1 wt % at room temperature and 20 bar.[18,20] The low hydrogen uptake at room temperature is the main disadvantage for the use of organometallic materials as adsorbents. With the advent of nanotechnology, carbon-based materials, including nanotubes, nanofibers, and activated carbon materials, have been analyzed experimentally and theoretically.[6−13,21−23] However, as a result of weak interactions between H_2 and pure carbon, these materials do not show sufficient storage capacity for commercial use under room temperature working conditions.

Since Chen et al.[24] reported that alkali-metal-doped carbon nanotubes exhibit remarkable hydrogen uptake, a great deal of experimental and theoretical work has been done to investigate the hydrogen adsorption in metal-doped carbon materials.[25−31] These studies showed that charge transfer from the alkali metal to these carbon materials polarize hydrogen molecules. As a result, a charge-induced dipole moment enhances the adsorption of hydrogen at ambient conditions. Besides, doping also increases the space to bind additional amounts of H_2.[30]

We have recently reported hydrogen adsorption on corannulene, a bowl-shaped molecule[32] with higher electron density in peripheral-carbon atoms than in inner-carbon atoms.[33] MP2 calculations yielded binding energies in the range −0.94 to −0.83 kcal/mol between a single hydrogen molecule and corannulene, depending on the adsorption site.[33] Molecular dynamics (MD) simulations of crystalline corannulene predicted about 0.79 wt % of H_2 at 72 bar at 273 K and 0.68 wt % at 300 K, in very good agreement with experimental results.[33] On the basis of MD simulations of corannulene stacks with different interlayer separations, we observed that the main factors that affect the hydrogen uptake capacity include the pressure applied to the system, temperature of adsorption, and the available space in the adsorbent assembly. For corannulene molecules arranged in stacks, it was observed that, as the interlayer distance (ILD) increases, the hydrogen uptake increases significantly. Thus, the adsorption of an alkali metal may enhance H_2 storage, not only due to the induction of dipole moments but also because of the generation of additional available space for H_2 storage.

Experimentally, ball milling has been proved to effectively increase the lithium doping concentration in carbon materials, and this technique is ready to be extended to industrial scales.[34] Kang[35] found the stable complex of pyrene−Li_4 where the ratio of Li to C is 1:4. Deng et al.[30] found that the most stable ratio

* Corresponding author. E-mail: balbuena@tamu.edu.
[†] Department of Chemical Engineering, Texas A&M University.
[‡] Air Force Research Laboratory, Energy Storage & Thermal Sciences Branch, Wright-Patterson Air Force Base.

10.1021/jp063963e CCC: $33.50
Published on Web 10/13/2006

of Li:C is 1:6 and 1:8 for Li−graphite intercalation compound (Li−GIC) at its equilibrium interlayer distance, while it is 1:3 for Li−pillared graphene sheet (Li−PGS) for interlayer separations greater than 8 Å. In this paper, we report ab initio and density functional theory (DFT) studies of the doping of lithium atoms to the corannulene molecule as well as on its interactions with H_2. We also analyze the effect that doping of Li atoms to corannulene has on H_2 uptake capacity at finite temperatures and pressures using classical MD simulations. We investigate two types of structures, one with six lithium atoms doped on a single corannulene molecule and the other with five lithium atoms, which leads to Li to C ratios between 1:3 and 1:4, consistent with results from other groups.[30,35]

2. Computational Methods

2.1. Ab Initio and DFT Calculations. The Gaussian 03 package[36] was used to undertake the molecular orbital theory calculations. Previous theoretical studies on corannulene indicated that a hybrid DFT method combined with double-ξ plus polarization basis sets would well reproduce the structural parameters of corannulene[37,38] and protonation and lithium cation binding on corannulene.[32,39] In this paper, we use B3LYP/6-31g(d,p) for geometry optimization of lithium-atom-doped corannulene complexes and B3LYP/6-311g(d,p) for potential energy surface scans. The optimized geometries are followed by frequency calculations to prove that the stationary points are local minima and find the zero point energy corrections. Single point calculations and full optimizations using second-order Möller−Plesset perturbation theory (MP2) with the 6-31G-(d,p) basis set are performed to obtain more accurate binding energies accounting for weak van der Waals forces that are responsible for the H_2/corannulene interaction based on physisorption.

2.2. Classical MD Simulations. The derivation of the force fields for H_2−corannulene interactions was reported previously.[33] Lennard-Jones (LJ) parameters were derived using the LJ parameters for the Li atom, $D_{Li-Li} = 0.025$ kcal/mol, and $x_{Li-Li} = 2.451$ Å,[40] corresponding to the form:

$$E_{vdw} = D_{IJ}\left\{-2\left[\frac{x_{IJ}}{x}\right]^6 + \left[\frac{x_{IJ}}{x}\right]^{12}\right\} \quad (1)$$

These parameters and eq 1 were used to generate a new set of parameters according to the equivalent form

$$E_{vdw} = 4\epsilon\left\{\left[\frac{\sigma_{IJ}}{r}\right]^{12} - \left[\frac{\sigma_{IJ}}{r}\right]^{6}\right\} \quad (2)$$

yielding $\epsilon_{LiLi} = 0.0275$ kcal/mol and $\sigma_{LiLi} = 2.18$ Å. The Lorentz−Berthelot mixing rules were used to obtain the LJ cross parameters $\epsilon_{Li-H} = 0.0432$ kcal/mol and $\sigma_{Li-H} = 2.57$ Å. For the dipole-induced interaction, the dipole moment of the Li_3−$C_{20}H10$−Li_2 complex (3.856 D) calculated at the level of B3LYP/6-311G(d,p) and the Li polarizability of 2.43×10^{-23} cm^3 (ref 41) were used to define an average pair interaction calculated as:

$$\bar{\Gamma}_{ij} = -\frac{7759.74}{r^6}\,\text{meV} \quad (3)$$

The dipole-induced interaction between Li and H_2 (equation 3) was added to eq 2 to generate new data using the nonbonded interaction parameters $\epsilon_{Li-H} = 0.0432$ kcal/mol and $\sigma_{Li-H} = 2.57$ Å, and a new fitting of these data to the form of the LJ eq 2 yielded $\epsilon_{Li-H} = 0.9$ kcal/mol and $\sigma_{Li-H} = 2$ Å, which are the parameters used in the MD simulations.

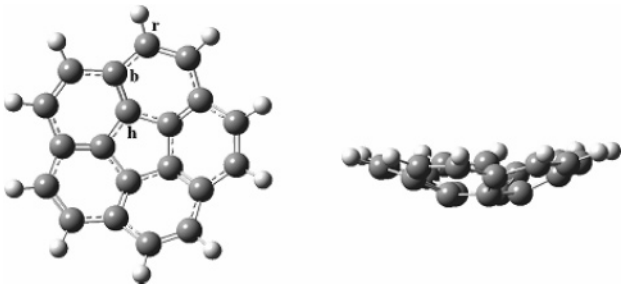

Figure 1. Optimized structure of corannulene at the level of B3LYP/6-311G(d,p).

TABLE 1: DFT(B3LYP/6-311G(d,p)) Structural Parameters and Mulliken Charge Distribution in Corannulene[a]

atom	charge	atom pair	bond distance (Å)	angle (deg)	
C_h	−0.04	C_h-C_h	1.42	$C_h-C_h-C_b$	122.88
C_b	0.00	C_h-C_b	1.38	$C_h-C_b-C_r$	114.43
C_r	−0.07	C_b-C_r	1.45	$C_b-C_r-C_r$	121.96
H	+0.09	C_r-C_r	1.40	$C_r-C_b-C_r$	129.78

[a] The atomic charges are average values.

The DL_POLY program,[42] version 2.14, was used for all MD simulations. A cutoff value of 10 Å was used for nonbonded interactions, and periodic boundary conditions in three dimensions were applied to the simulation cell. The simulations were run in the canonical *NVT* ensemble at temperatures of 273 K and 300 K and pressures up to 250 bar. Details of the assembled system are provided in the Results and Discussion Section. The total simulation time for each *P* and *T* is 800 ps, with 300 ps for the equilibration period and 500 ps for the production period. The evaluations of H_2 uptake are based on the 500 ps production period.

3. Results and Discussion

3.1. Doping of Li Atoms to Corannulene. Corannulene is a bowl-shape molecule with C_{5v} symmetry. Figure 1 shows the structure of corannulene optimized at the level of B3LYP/6-311G(d,p). There are three types of carbon atoms: the outmost 10 carbons bonded to one hydrogen each are named as "rim" carbons (C_r), the innermost five carbons on the five-membered ring as "hub" carbons (C_h), while the remaining five carbons connecting between the rim and hub carbon atoms are designated as "bridge" carbons (C_b).

The calculation shows that rim carbon atoms possess higher electron density than hub and bridge carbon atoms, thus the dipole vector would point toward the five-membered ring. The calculated dipole moment of corannulene is 2.18 D, which is close to the experimental data of 2.07 D.[43] The structural information and Mulliken charge distribution of corannulene are shown in Table 1.

Recent DFT studies[35] of Li−aromatic sandwich compounds, R−nLi−R, where R is benzene, naphthalene, or pyrene, reported that the Li atom was preferentially adsorbed over the six-membered ring instead of over individual or pairs of C atoms. For a single Li ion, it was found that the Li cation was bounded on the convex side over a six-membered ring of corannulene at the level of B3LYP/6-311G(d,p)//B3LYP/6-31G(d,p).[32] The data in Table 2 indicate that complexation of a Li ion at the convex side is more stable than at the concave side, which is in agreement with the results of Frash et al.,[32] whereas, for the Li atom, complexation at the concave side is more stable (by 1.2 kcal/mol) than at the convex side.

TABLE 2: Structural and Energetic Properties and Mulliken Charges in Complexes of Corannulene with a Lithium Cation/ Atom Attached to a Six-Membered Ring, Optimized at the B3LYP/6-31G(d,p) Level

complex with corannulene	Li−C distance (Å)	electronic energy (hartrees)	binding energy (kcal/mol)	charges on atoms (e)			
				Li	C_r	C_b	C_h
Li^+ on the concave side	2.28−2.31	−775.52514	−47.5	0.44	−0.12	0.12	−0.03
Li^+ on the convex side	2.29−2.44	−775.52700	−48.7	0.46	−0.13	0.15	−0.06
Li on the concave side	2.22−2.25	−775.68264	−16.8	0.33	−0.15	0.11	−0.05
Li on the convex side	2.14−2.38	−775.68073	−15.6	0.31	−0.16	0.17	−0.08

The Mulliken charges on the various atoms (labels as in Figure 1) shown in Table 2 suggest that the higher charge of the Li cation may be the reason for the stronger binding to the corannulene molecule.

Multiple Li atoms can be adsorbed either at the concave or at the convex side. Figure 2 shows attachment of five Li atoms on corannulene at the level of B3LYP/6-31G(d,p). Considering the effect of charge transfer from Li to C atoms and thus the repulsion between two positively charged lithium atoms, the initial geometries were arranged with Li atoms over the outer six-membered rings on either side. In the initial configuration, all five Li atoms were located at the same side (either convex or concave) of the corannulene molecule, and the optimized structure resulted always with the five Li atoms attached to the concave side, over the six-membered rings, as shown in Figure 2a. Thus, when the optimization was started locating the Li atoms over the convex side, there was an inversion of curvature of the corannulene molecule, in agreement with the tendency shown in Table 2 for a single Li atom. Similarly, when the initial configuration contains two Li atoms on one side and three on the other side, the energetically favorable optimized conformations contain more Li atoms on the concave side, that is, three Li atoms on the concave side and the other two Li atoms on the convex side (Figure 2b); this conformation has lower energy than that in Figure 2a by minimizing repulsion effects. Frequency calculations indicate that both complexes in Figure 2 are local minima.

Comparison of the respective energies is shown in Table 3, along with related structural information. The $Li_5-C_{20}H_{10}$ and $Li_3-C_{20}H_{10}-Li_2$ complexes have σ_v symmetry, as shown in Figure 2. Table 3 illustrates that there is charge transfer from Li atoms to corannulene molecules, resulting in positive charges on Li atoms of $Li_5-C_{20}H_{10}$ and $Li_3-C_{20}H_{10}-Li_2$. Overall, the total charge on Li atoms in $Li_3-C_{20}H_{10}-Li_2$ is higher than those in $Li_5-C_{20}H_{10}$. Thus, C atoms of corannulene are more negatively charged in the first complex, resulting in higher electrostatic interaction and shorter distances from Li atoms to six-membered rings of corannulene in $Li_3-C_{20}H_{10}-Li_2$ than in $Li_5-C_{20}H_{10}$.

Each of the three Li atoms (1Li, 4Li, and 5Li) on the concave side of $Li_3-C_{20}H_{10}-Li_2$ locate close to the center of a six-membered ring, whereas the two attached to the convex side of $Li_3-C_{20}H_{10}-Li_2$ are closer to a six-membered ring than those on the concave side of $Li_5-C_{20}H_{10}$. The calculated energies show that $Li_3-C_{20}H_{10}-Li_2$ is about 4 kcal/mol more stable than $Li_5-C_{20}H_{10}$; the binding energy per Li atom is −23.91 kcal/mol-Li in $Li_3-C_{20}H_{10}-Li_2$ and −23.11 kcal/mol-Li in $Li_5-C_{20}H_{10}$.

The doping of six Li atoms on corannulene is illustrated in Figure 3, which shows four different combinations tested on the basis of the results obtained for complexes with five Li atoms. Figure 3a displays the complex $Li_6-C_{20}H_{10}$, where the first five Li atoms are doped over six-membered rings on the concave side, and the sixth lithium atom is in the center over these five Li atoms. Alternatively, with the sixth Li atom doped at the convex side, we obtain the $Li_5-C_{20}H_{10}-Li$ complex (Figure 3b). Both $Li_6-C_{20}H_{10}$ and $Li_5-C_{20}H_{10}-Li$ have σ_v symmetry, with the atoms labeled 1Li and 6Li located on the

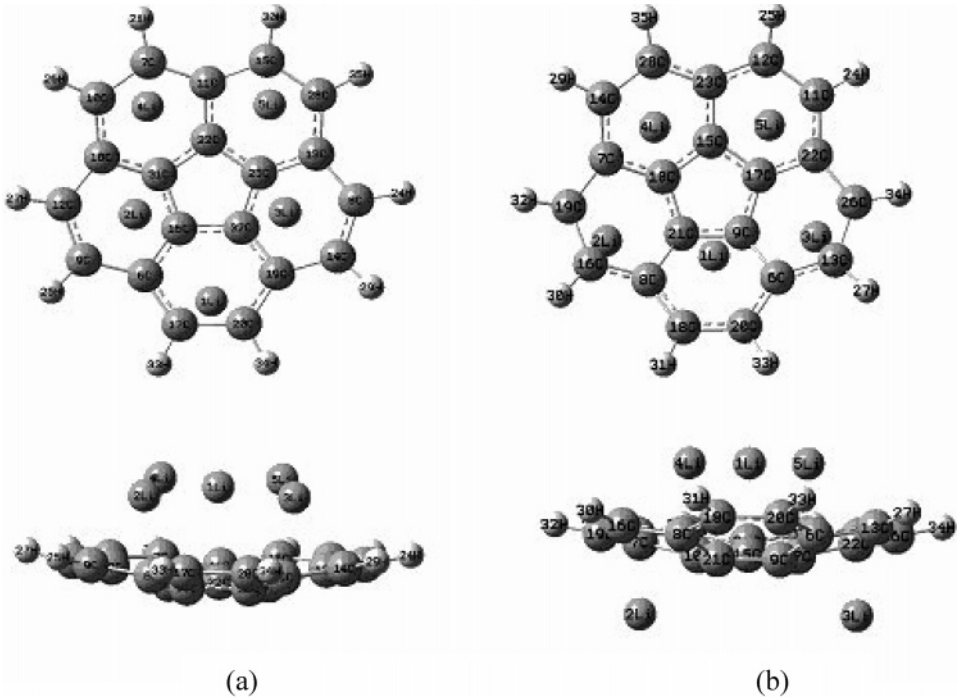

Figure 2. Optimized (B3LYP/6-31G(d,p)) conformations of corannulene complexed with five Li atoms doped at different positions. (a) Five Li atoms doped at the concave side over six-membered rings, $Li_5-C_{20}H_{10}$. (b) Three lithium atoms doped at the concave side and two at the convex side over six-membered rings, $Li_3-C_{20}H_{10}-Li_2$.

TABLE 3: Li-Doped Corannulene Complexes: Structural Information and Electronic Energy (Ha) and Binding Energy (kcal/mol of Li) at the Level of B3LYP/6-31G(d,p)

complex	Li label (as shown in Figure 2)	charge of Li (e)	distance Li−C (Å)[a]		
			Li−C_r	Li−C_b	Li−C_h
$Li_5-C_{20}H_{10}$	1	0.32	2.14	2.65	3.07
	2, 3	0.14	2.23, 2.24	2.30, 2.33	2.32, 2.34
	4, 5	0.25	2.14, 2.17	2.51, 2.55	2.82, 2.86
$Li_3-C_{20}H_{10}-Li_2$	1	0.45	2.21	2.29	2.36
	2, 3	0.48	2.13, 2.19	2.27, 2.53	2.18, 2.41
	4, 5	0.22	2.13, 2.22	2.25, 2.47	2.42, 2.51

	electronic energy (Ha)	zero point energy (Ha)	binding energy (kcal/mol of Li)
Li	−7.49098		
$C_{20}H_{10}$	−768.16483	0.23195	
$Li_5-C_{20}H_{10}$	−805.80384	0.23366	−23.11
$Li_3-C_{20}H_{10}-Li_2$	−805.81022	0.23260	−23.91

[a] When two values are shown, each one represents two pairs of the distance of Li−C in σ_v complexes.

TABLE 4: Li−Corannulene Complexes: Structural Information, Electronic Energy (Ha), and Binding Energy Per Li Atom (kcal/mol-Li) at the Level of B3LYP/6-31G(d,p)[a]

complex	Li label (shown in Figure 3)	Li charge	distance Li−C (Å)		
			Li−C_r	Li−C_b	Li−C_h
$Li_6-C_{20}H_{10}$	1	0.22	2.16	2.67	3.16
	2, 3	0.31	2.19,2.20	2.27, 2.31	2.34, 2.36
	4, 5	0.26	2.14, 2.18	2.55, 2.64	2.97, 3.02
	6	−0.23	5.08	4.76	4.55
$Li_5-C_{20}H_{10}-Li$	1	0.45	2.10	2.57	3.05
	2, 3	0.14	2.17, 2.22	2.31, 2.40	2.43, 2.44
	4, 5	0.21	2.07, 2.15	2.46, 2.49	2.75, 2.79
	6	0.51	2.15	2.42	2.25
$Li_4-C_{20}H_{10}-Li_2$	1	0.26	2.22, 2.28	2.33, 2.45	2.44, 2.52
	2	0.47	2.14, 2.19	2.27, 2.51	2.21, 2.33
	3	0.45	2.12, 2.13	2.36, 2.43	2.24, 2.31
	4	0.15	2.23, 2.37	2.23, 2.55	2.37, 2.51
	5	0.05	2.18, 2.18	2.51, 2.52	2.81, 2.84
	6	0.49	2.149,2.157	2.518,2.585	2.92, 2.98
$Li_3-C_{20}H_{10}-Li_3$	1	0.30	2.32, 2.37	2.35, 2.46	2.36, 2.42
	2	0.45	2.17, 2.22	2.31, 2.50	2.21, 2.33
	3	0.20	2.13, 2.25	2.26, 2.63	2.24, 2.46
	4	0.15	2.17, 2.28	2.29, 2.54	2.50, 2.65
	5	0.35	2.17, 2.39	2.31, 2.62	2.57, 2.75
	6	0.39	2.17, 2.17	2.40, 2.41	2.29, 2.32

	electronic energy (Ha)	zero point energy (Ha)	binding energy (kcal/mol-Li)
Li	−7.49098		
$C_{20}H_{10}$	−768.16483	0.23195	
$Li_6-C_{20}H_{10}$	−813.35008	0.23616	−25.03
$Li_5-C_{20}H_{10}-Li$	−813.34599	0.23443	−24.61
$Li_4-C_{20}H_{10}-Li_2$	−813.34763	0.23374	−24.78
$Li_3-C_{20}H_{10}-Li_3$	−813.33568	0.23309	−23.53

[a] Each value in σ_v symmetry complexes, $Li_6-C_{20}H_{10}$ and $Li_5-C_{20}H_{10}-Li$, represents two pairs of the distance of Li−C.

symmetry plane. Another complex contains the first five Li atoms doped as in the complex $Li_3-C_{20}H_{10}-Li_2$, and the sixth Li atom is attached either to the concave or to the convex side over a six-membered ring, forming $Li_4-C_{20}H_{10}-Li_2$ (Figure 3d) and $Li_3-C_{20}H_{10}-Li_3$ (Figure 3c). These complexes are no longer symmetric after optimization. Frequency calculations on the optimized structures of these complexes also indicate they are local minima, except for $Li_5-C_{20}H_{10}-Li$, which is a saddle point.

Table 4 summarizes partial structural and energetic information. The most important difference is the negative charge over the Li atom on top of $Li_6-C_{20}H_{10}$, which may favor electrostatic Li−Li interactions, resulting in $Li_6-C_{20}H_{10}$ being 9 kcal/mol more stable than $Li_3-C_{20}H_{10}-Li_3$. The binding energies per mole of Li are −25.03 and −23.53 kcal/mol-Li for $Li_6-C_{20}H_{10}$ and $Li_3-C_{20}H_{10}-Li_3$, respectively. The relatively large binding energies of the Li_6 and Li_5 complexes of corannulene might indicate stable Li adsorption on corannulene, with the ratio of Li:C between 1:4 and 1:3. The lithium doping concentration is in agreement with results reported by other groups.[30,35]

3.2. Adsorption of H_2 on Li-Doped Corannulene Complexes. *3.2.1. $Li_6-C_{20}H_{10}$ and $Li_5-C_{20}H_{10}-Li.$* Adsorption of H_2 is studied on the most stable complexes at each doping concentration, i.e., on $Li_6-C_{20}H_{10}$ and on $Li_3-C_{20}H_{10}-Li_2$. To obtain a qualitative comparison of the interaction strengths of H_2 in corannulene and Li-doped corannulene, we computed a potential energy scan, as shown in Figure 4, which illustrates that no attractive interactions between hydrogen and the corannulene molecule are detected at this level of theory when a head-on H_2 molecule approaches the corannulene molecule

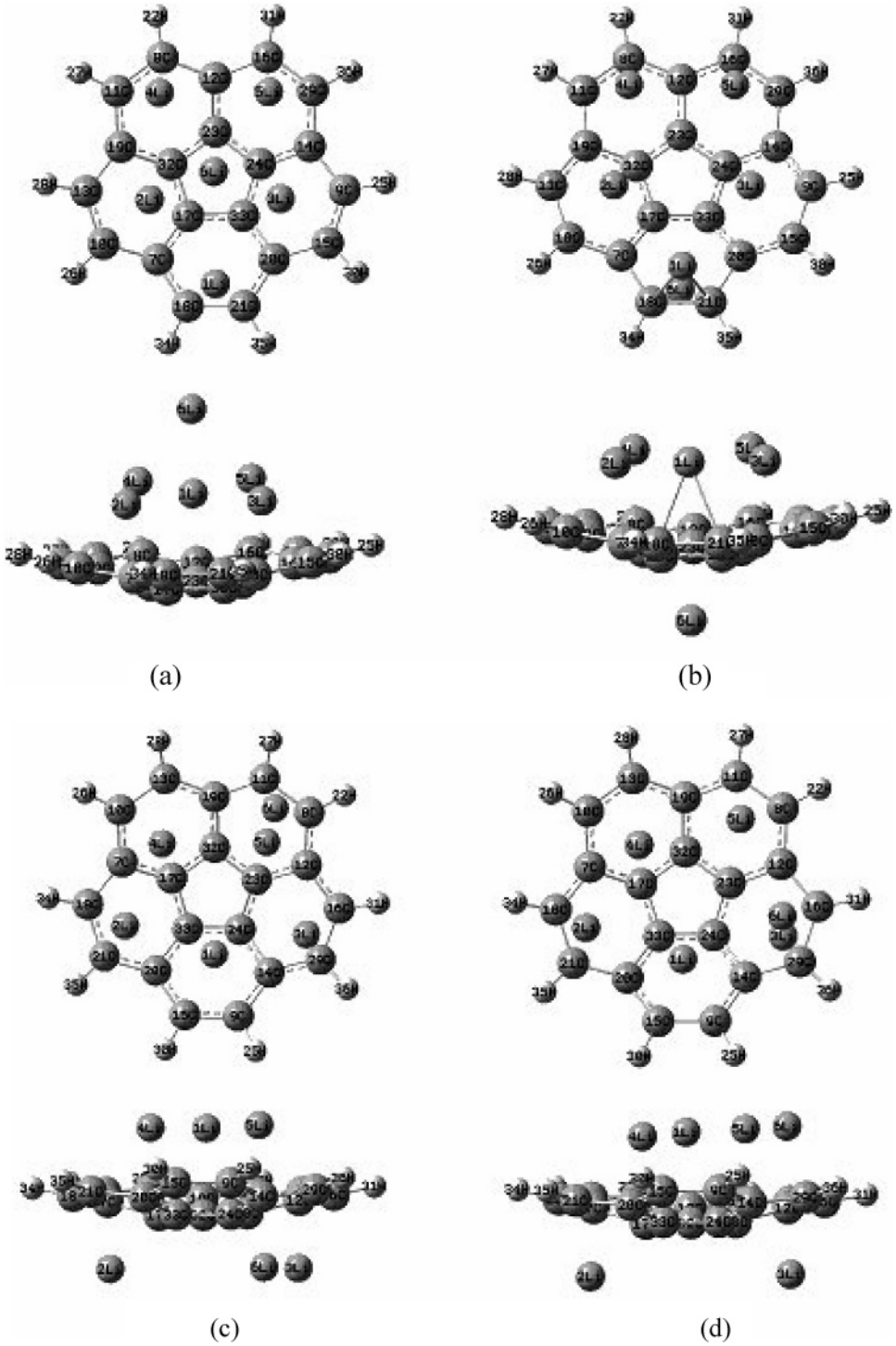

Figure 3. Optimized (B3LYP/6-31G(d,p)) conformations of corannulene with six Li atoms. (a) Six Li atoms doped at the concave side, $Li_6-C_{20}H_{10}$. (b) Five Li atoms doped at the concave side and one at the convex side, $Li_5-C_{20}H_{10}-Li$. (c) Three Li atoms doped at the concave side and three at the convex side, $Li_3-C_{20}H_{10}-Li_3$. (d) Four Li atoms doped at the concave side and two at the convex side, $Li_4-C_{20}H_{10}-Li_2$.

along pathways a, b, c, and d (Figure 4). However, when H_2 approaches $Li_6-C_{20}H_{10}$ (pathway e) or $Li_3-C_{20}H_{10}-Li_2$ (pathway f), a relatively strong attractive interaction between H_2 and the Li atom−corannulene complex is observed. The strongest attraction appeared when the center of mass of the H_2 molecule is at a distance of 2.47 Å from the corresponding Li atom (Figure 5), yielding binding energies of −0.47 and −2.06 kcal/mol with $Li_6-C_{20}H_{10}$ and $Li_3-C_{20}H_{10}-Li_2$, respectively. Figure 5 shows the structures of H_2 interacting with $Li_6-C_{20}H_{10}$ and $Li_3-C_{20}H_{10}-Li_2$ at the geometries corresponding to the minima on the potential surface curves of Figure 4. The separation of 2.47 Å (Figure 5) corresponds to a distance of 2.10 Å, shown in Figure 4, because that is the distance between the closest H atom and the corresponding Li atom; the difference between them is one-half of the calculated bond distance of H_2 (0.74 Å).

To account for weak van der Waals forces that are responsible for the H_2/Li−corannulene complex interactions, we use second-order Moller−Plesset perturbation theory to determine the energy corresponding to such geometries using the 6-31G(d,p) basis set. The calculated MP2/6-31G(d,p) energies (single point calculations) are −1.83 and −2.82 kcal/mol for the H_2-Li_6-

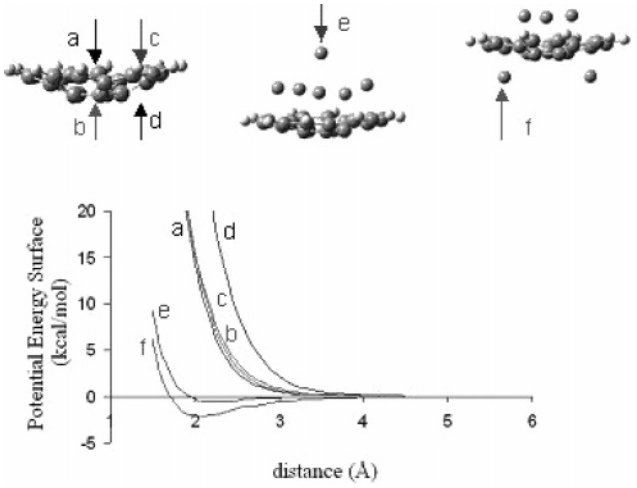

Figure 4. Potential energy surface of H_2 approaching corannulene and lithium-doped corannulene at the level of B3LYP/6-311G(d,p); in each curve, H_2 approaches corannulene at: (a) the center five-membered ring at the concave side, (b) the center five-membered ring at the convex side, (c) the center of a six-membered ring at the concave side, (d) the center of a six-membered ring at the convex side, (e) the top Li atom in $Li_6-C_{20}H_{10}$ (see Figure 3), (f) the Li atom on the convex side in $Li_3-C_{20}H_{10}-Li_2$ (see Figure 2).

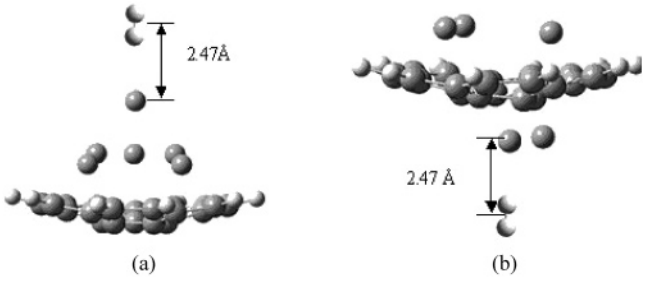

Figure 5. Structures corresponding to the minima in the potential energy scans: (a) $Li_6-C_{20}H_{10}$, (b) $Li_3-C_{20}H_{10}-Li_2$.

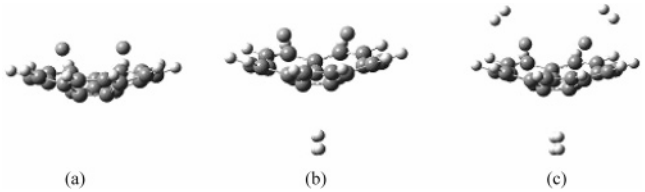

Figure 6. Optimized configurations of H_2 adsorption on $Li_2-C_{20}H_{10}$, with MP2(FC)/6-31G(d): (a) $Li_2-C_{20}H_{10}$; (b) $2H_2-(Li_2-C_{20}H_{10})$; (c) $4H_2-(Li_2-C_{20}H_{10})$.

$C_{20}H_{10}$ system and $H_2-Li_3-C_{20}H_{10}-Li_2$, respectively. Recently, we reported binding energies of −0.94 and −0.83 kcal/mol for the physisorption of H_2 on corannulene using MP2(full)/6-31G-(d) for H_2 on the concave side and the convex side, respectively.[33] Thus, the H_2-Li interaction is stronger than that between H_2 and C based on these binding energies. In the next section, we refine these estimates using optimizations with the MP2 method.

3.2.2. $Li_2-C_{20}H_{10}$. In this section, we analyze the most favorable hydrogen adsorption sites using $Li_2-C_{20}H_{10}$ (Figure 6a), first with two hydrogen molecules on the convex side (Figure 6b) and then with two hydrogen molecules on the convex side and two hydrogen molecules on the concave side (a total of four H_2 molecules, Figure 6c). The optimized configurations of these systems at the MP2(FC)/6-31G(d) level have a symmetry plane, and the two H_2 molecules adsorbed on the convex side are located on that plane (Figure 6b and c),

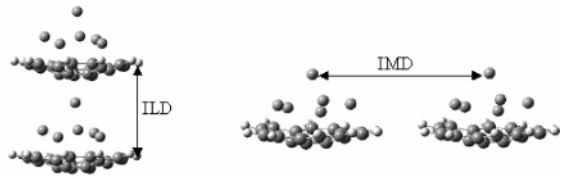

Figure 7. Definition of interlayer distance (ILD) and intermolecular distance (IMD).

one molecule is adsorbed over the five-membered ring, and the other over a six-membered ring, and each of the lithium atoms is located over a six-membered ring. For the H_2 molecule adsorbed over the five-membered ring, the distance between the closer H atom to hub carbons is in the range of 3.13−3.24 Å, while the H_2 molecule over the six-membered ring is closer to the pair of hub carbon atoms in the center, with a distance in the range of ∼3.18 Å. Two additional H_2 molecules adsorbed on the concave side (Figure 6c) adsorb on lithium atoms; the shortest H−Li distance is ∼2.12 Å, significantly shorter than the distance between H_2 molecules (on the convex side) and carbon atoms.

The difference between adsorption distances on the various sites suggests that the Li atoms are the most favorable sites for hydrogen adsorption, which is confirmed by the calculated binding energies. For H_2 adsorbed on the convex side (Figure 6b), a binding energy of −0.92 kcal/mol-H_2 is obtained. On the basis of the similar geometry of these two adsorbed H_2 molecules in Figure 6b and c, we assume that the binding energy of these two H_2 molecules are the same in the two cases, thus we infer that a binding energy of −1.48 kcal/mol-H_2 corresponds to the interaction between H_2 (on the concave side) and a lithium atom. The energetic difference clearly shows that Li atoms are the favorable adsorption sites for H_2 molecules, suggesting a mechanism of enhanced hydrogen adsorption on lithium-atom-doped corannulene systems.

Another important feature in the Li-doped complexes of corannulene is the increase of the dipole moment. DFT predicts values of 5.39 and 3.86 D, respectively, for $Li_6-C_{20}H_{10}$ and $Li_3-C_{20}H_{10}-C_2$, whereas the MP2 calculation yields 3.47 D for the $Li_2-C_{20}H_{10}$ complex. The presence of this enhanced dipole in the molecule induces a dipole moment in the H_2 molecules, which is taken into account to define the effective force field (Section 2.2) for molecular dynamics simulations discussed in the next section.

3.3. Adsorption at Finite Temperatures and Pressures. *3.3.1. Arrangement of Adsorbent Molecules.* To investigate the available space and collective effects on H_2 adsorption, we assume that lithium-doped corannulene molecules arrange in a stack configuration. In this case, we can adjust the interlayer and intermolecular distances (as defined below), performing analyses similar to those reported by other researchers using carbon nanotube bundles and graphite nanofibers.[30,44−46] Each MD simulation cell contains 16 lithium-atom-doped corannulene molecules, with eight molecules in each layer located at the bottom of the cell. In the MD simulations, the dynamics of the adsorbent molecules is not included, thus the adsorbent molecules are kept fixed in their initial positions and their distribution in each layer is determined by two parameters, the interlayer distance, ILD, and the intermolecular distance, IMD. The ILD is defined as the distance between two overlapped molecules and the IMD is the separation between the centers of two parallel molecules, as shown in Figure 7. The values of IMD and ILD were determined from DFT calculations discussed in the next section.

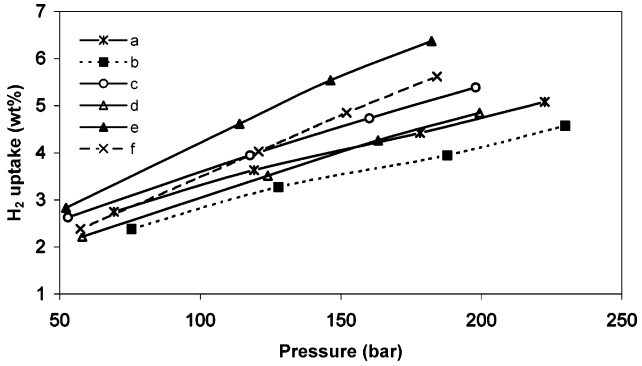

Figure 8. Calculated hydrogen uptake capacity of $Li_6-C_{20}H_{10}$ molecules assembled in stacks. (a) ILD = 6.5 Å, 273 K; (b) ILD = 6.5 Å, 300 K; (c) ILD = 8 Å, 273 K; (d) ILD = 8 Å, 300 K; (e) ILD = 10 Å, 273 K; (f) ILD = 10 Å, 300 K.

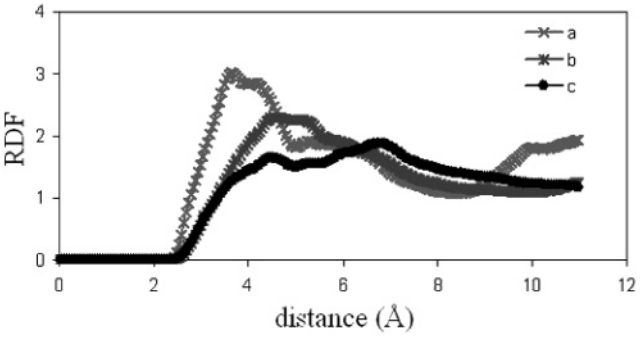

Figure 9. Radial distribution function of pairs $C-H_2$ for the adsorption of H_2 in stacks of the $Li_6-C_{20}H_{10}$ complex at 273 K: (a) ILD = 6.5 Å, P = 119 bar, and H_2 uptake of 3.63 wt %; (b) ILD = 8 Å, P = 118 bar, and H_2 uptake of 3.95 wt %; (c) ILD = 10 Å, P = 114 bar, and H_2 uptake of 4.61 wt %.

3.3.2. Estimation of the IMD and ILD Parameters. DFT partial optimizations at the level of B3LYP/6-311G(d,p) are performed for the characterization of the ILD and IMD distances in dimers of $Li_6-C_{20}H_{10}$, as shown in Figure 7. To determine the optimum ILD value, only the z coordinates of the dimer are allowed to change, whereas only the x coordinates of the dimer are allowed to change to investigate the optimum IMD value. The results are 11.4 Å for the IMD and 6.5 Å for the ILD. In our MD simulations, the IMD is fixed to 11.0 Å for all the adsorbent systems, and additional values of ILD of 8.0 and 10.0 Å are used for a simple stack of two different lithium-doped corannulene systems. Such a system is chosen to investigate the potential H_2 uptake capacity, assuming that substitution of H with bulky alkyl function groups to the rim carbons or bridging of lithium-atom-doped corannulene molecules might be used to increase the ILD.

3.3.3. Hydrogen Adsorption on Lithium-Doped Corannulene. Figure 8 shows the predicted H_2 uptake at 273 and 300 K and various ILD for $Li_6C_{20}H_{10}$ as a function of H_2 pressure. Overall, the MD simulations predict: (1) at all the conditions studied, the H_2 uptake is higher than 2 wt %; (2) the H_2 uptake at a given ILD and temperature is almost linear with the increase of pressure; (3) adsorption decreases as temperature increases; (4) increasing ILD while keeping the same T and P significantly increases the H_2 uptake, and the change is especially notorious increasing the ILD from 8.0 to 10.0 Å. At the estimated equilibrium separation ILD of 6.5 Å, the predicted H_2 uptake values are 2.75−5.08 wt % at 70 and 225 bar at 273 K, whereas at 300 K, the values are reduced to 2.38−4.58 wt % at 75 and 230 bar, respectively (Figure 8). Thus, according to the projection, the H_2 uptake at an ILD of 6.5 Å would reach 6.5 wt % at 300 K and 315 bar.

Parts c−f of Figure 8 illustrate that the rate of increase of H_2 uptake (i.e., the slope of the lines in Figure 8) increases as the interlayer distance increases at the same conditions of temperature and pressure, yielding significantly enhanced uptake at higher pressures for higher ILD separations. This could be attributed to the distribution of hydrogen molecules between adsorbent molecules, as seen from radial distribution functions (RDFs) between C and H_2, shown in Figure 9.

At an ILD of 6.5 Å, a relatively sharp peak is observed at a distance between 3.5 and 4.5 Å, with a shoulder appearing at about 5 Å. This fairly sharp peak indicates that the majority of the H_2 molecules located between adsorbent molecules are distributed in a relatively thin layer, possibly interacting with the Li atom on top, whereas the shoulder may correspond to the molecules in a second layer located in the intermolecular space.

As the ILD increases to 8 Å, a broader peak (Figure 9) covers a distance between 4.0 and 7 Å, which reveals the larger space accessible to hydrogen molecules and the thickening of the adsorption layer. These features are clearly illustrated in Figure 10. At an ILD of 10 Å, two broad (overlapping) peaks are evident in Figure 9, centered in ∼4 and ∼7Å respectively, corresponding to the formation of two adsorption layers of hydrogen molecules between adsorbent molecules.

The formation of two adsorption layers might explain the large increase in H_2 uptake when the ILD increases from 8 to 10 Å. Similar H_2 distribution has been found in single-wall and double-wall carbon nanotubes, and especially in GNFs as the VDW gaps increase in these systems.[44] According to our

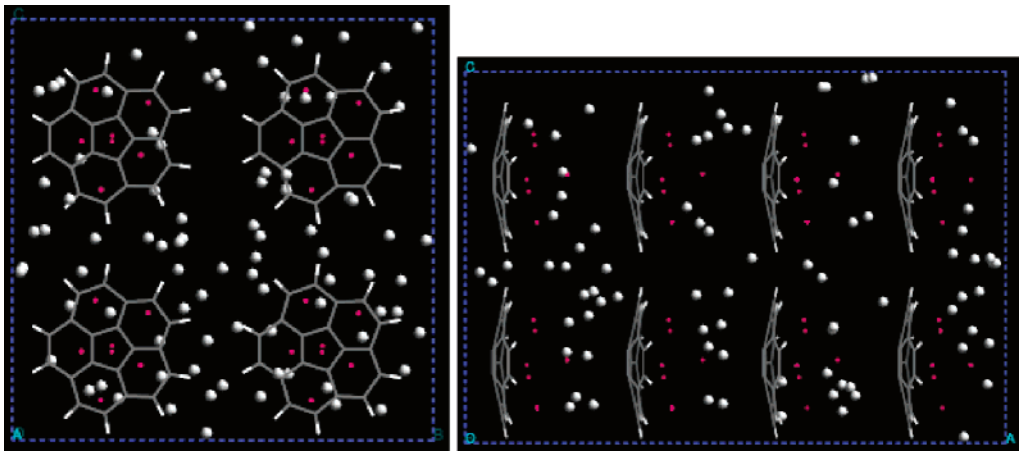

Figure 10. Snapshots of $Li_6-C_{20}H_{10}$ systems of adsorbent layers with hydrogen adsorbed at ILD = 8 Å, 300 K, and 124 bar.

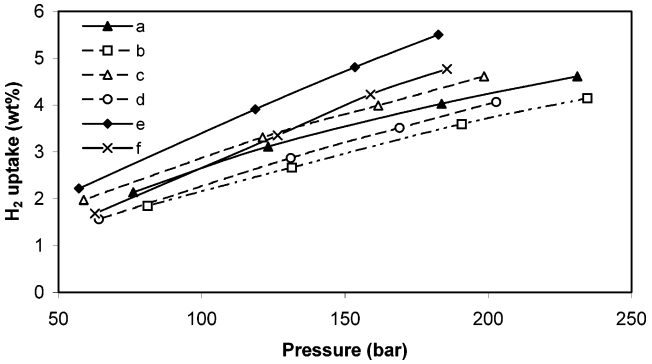

Figure 11. Hydrogen uptake capacity of $Li_3-C_{20}H_{10}-Li_2$. (a) ILD = 6.5 Å, 273 K; (b) ILD = 6.5 Å, 300 K; (c) ILD = 8 Å, 273 K; (d) ILD = 8 Å, 300 K; (e) ILD = 10 Å, 273 K; (f) ILD = 10 Å, 300 K.

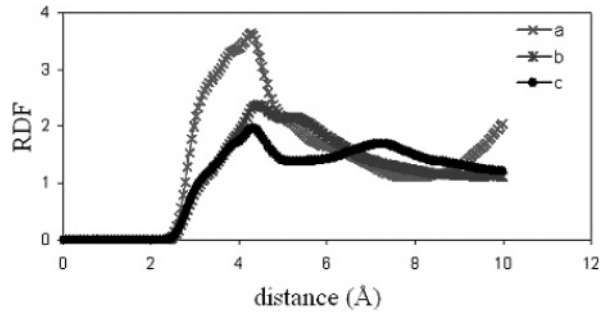

Figure 12. Radial distribution function of $C-H_2$ in the $Li_3-C_{20}H_{10}-Li_2$ complex: (a) ILD = 6.5 Å, 273 K, P = 123 bar, and H_2 uptake of 3.11 wt %; (b) ILD = 8 Å, 273 K, P = 121 bar, and H_2 uptake of 3.31 wt %; (c) ILD = 10 Å, 273 K, P = 119 bar, and H_2 uptake of 3.91 wt %.

predictions, for an ILD of 10 Å, it may be possible to reach the target 6.5 wt % at 215 bar and 300 K, or at 185 bar and 273 K.

To analyze the role that the Li concentration present in the Li−corannulene complexes has on the H_2 physisorption, we also study H_2 uptake on $Li_3-C_{20}H_{10}-Li_2$, arranged on stacks. Figure 11 shows the predicted H_2 uptake at 273 and 300 K and various ILD. The overall H_2 uptake behavior is similar to that found in stacks of $Li_6-C_{20}H_{10}$, including the almost linear response of H_2 uptake regarding to pressure, higher H_2 uptake at lower temperature, and higher rate of H_2 uptake at higher ILD. The corresponding RDFs of the $C-H_2$ pair shown in Figure 12 also suggest a relatively ordered adsorbed state. Details of the interactions are visualized in Figure 13.

Table 5 shows the comparison of H_2 uptake at 100 bar and various temperatures and ILDs for these Li-doped corannulene

TABLE 5: Comparison of H_2 Uptake at 100 Bar on Li-Doped Corannulene Systems[a]

ILD (Å)	273 K		300 K	
	$Li_6-C_{20}H_{10}$	$Li_3-C_{20}H_{10}-Li_2$	$Li_6-C_{20}H_{10}$	$Li_3-C_{20}H_{10}-Li_2$
6.5	3.26 (0.54)	2.63 (0.53)	2.78 (0.46)	2.17 (0.43)
8.0	3.56 (0.59)	2.81 (0.56)	3.03 (0.51)	2.24 (0.45)
10.0	4.19 (0.70)	3.38 (0.68)	3.49 (0.58)	2.65 (0.53)

[a] The number in parentheses is the ratio of the H_2 uptake to the number of Li atoms per corannulene molecule.

systems, illustrating that the difference of H_2 uptake (wt %) between the 6-Li and the 5-Li systems is about 0.61 to 0.84 at 100 bar; specific differences depend on the temperature and on the ILD values.

This difference may be caused by the lower lithium concentration in the five Li-doped corannulene systems, but also by the different distribution of electronic density between molecules in the two cases. Similar behavior of the dependence of H_2 uptake on lithium atom concentration was found in Li-pillared graphene sheets.[30] The ratio of the H_2 uptake to the number of Li atoms per corannulene molecule for each system at the same ILD, temperature, and pressure suggests a linear dependence of H_2 uptake on lithium doping concentration.

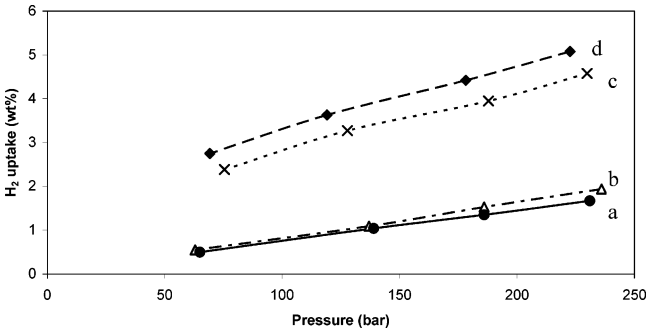

Figure 14. Comparison of hydrogen uptake on different adsorbent systems: (a) $C_{20}H_{10}$, ILD = 4.8 Å, 300 K; (b) $C_{20}H_{10}$, ILD = 4.8 Å, 273 K; (c) $Li_6-C_{20}H_{10}$, ILD = 6.5 Å, 300 K; (d) $Li_6C_{20}H_{10}$, ILD = 6.5 Å, 273 K.

Finally, Figure 14 shows a significant enhancement in the H_2 uptake in the Li-doped corannulene systems compared with those obtained with similar stacks of undoped corannulene;[33] in each case, the interlayer distance is that obtained via DFT geometry optimizations for the separation of two molecules arranged in a sandwich configuration.[33] This difference may be caused by the natural larger separation between corannulene molecules due to the presence of the Li atoms, by the higher

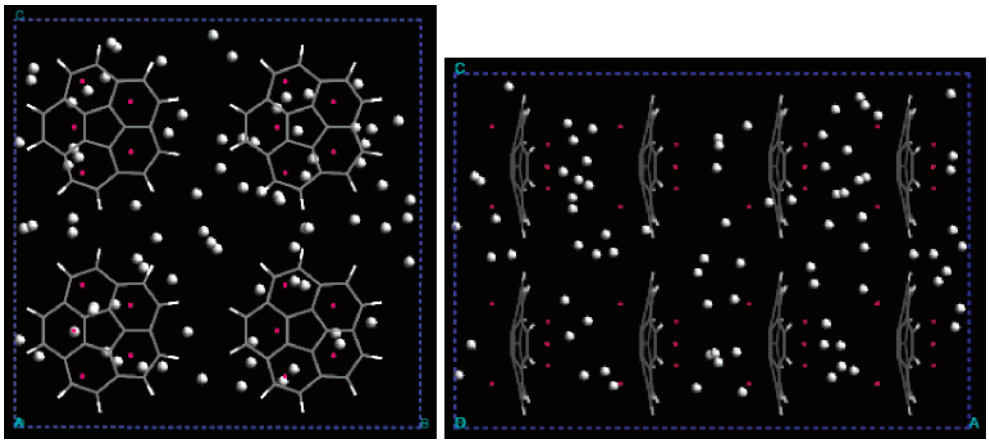

Figure 13. Snapshots of $Li_3-C_{20}H_{10}-Li_2$ systems of adsorbent layers with hydrogen adsorbed at ILD = 8 Å, 300 K, and 131 bar.

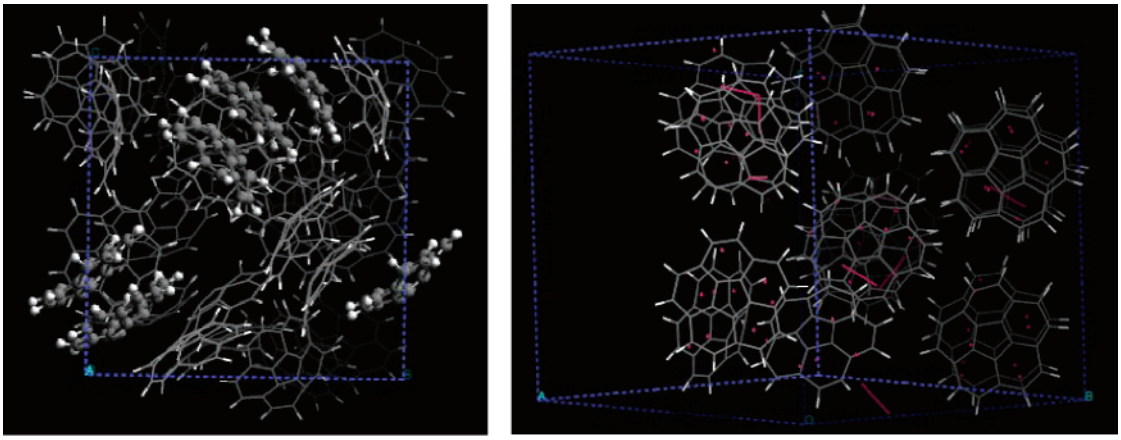

Figure 15. Bulk configurations of $C_{20}H_{10}$ (a) and $Li_3-C_{20}H_{10}-Li_2$ (b) at 300 K after MD simulations.

binding energy $Li-H_2$ compared to $C-H_2$, and by the dipole moment of the doped corannulene molecule, which induces polarization on H_2.

3.3.4. Discussion of the Effect of the Frozen Adsorbent. A valid question refers to the effect that our assumption of a frozen adsorbent might have on the adsorption results at finite pressures and temperatures shown in the previous sections. We have performed MD simulations of bulk $C_{20}H_{10}$ and $Li_3-C_{20}H_{10}-Li_2$ at 300 K, where the initial configurations corresponded to DFT fully optimized dimers arranged in stacks, but the molecules are not fixed. The first system (Figure 15a) contains 32 $C_{20}H_{10}$ molecules and the cell dimensions are $38.4 \times 22 \times 22$ Å^3 (initial IMD = 11 Å and ILD = 4.8 Å), whereas the second system (Figure 15b) contains 16 $Li_3-C_{20}H_{10}-Li_2$ molecules and the cell dimensions are $26 \times 22 \times 22$ Å^3 (initial IMD = 11 Å and ILD = 6.5 Å). These distributions and densities correspond to the adsorbent structures described in the previous sections; the difference is that the adsorbent phase is not fixed. The force field includes intra- and intermolecular interactions. Intramolecular interactions contain bond and valence angle interactions.[40] Intermolecular interactions include electrostatic terms with atomic charges assigned by the Mulliken results for dimers from DFT calculations at the level of B3LYP/6-311G(d,p) and van der Waals interactions with parameters as described in the computational methods section.

Snapshots after 800 ps shown in Figure 15 illustrate the formation of overlapped dimers or trimers, but the initial ideal stack arrangement is lost. Indeed, the two components of a corannulene dimer may arrange in T-shape and sandwich configurations with the T-shape being the most stable,[33,47] and semiempirical AM1 calculations using 4, 8, and 12 corannulene molecules yielded stable ensembles showing T-shape conformations.[47]

However, our previous results showed no significant differences for H_2 adsorption in fixed ensembles of T-shaped corannulene molecules versus stacked sandwiched configurations,[33] which motivated us to adopt the idealized stacked geometry in this study. Further investigations are needed to prove the adsorbent structure in the Li-doped systems.

4. Conclusions

Doping of lithium atoms to corannulene systems improves the hydrogen adsorption capacity due to increased dipole moment, large available space around the adsorbent molecules, and strong interactions between dopant and hydrogen molecules. The hydrogen uptake ability is also dependent on the concentration of lithium dopant.

A single Li atom is energetically more favorable when doped over a six-membered ring on the concave than on a convex side of corannulene. Doping of multiple Li atoms on the concave side is also more stable, with the number of Li atoms on the concave side exceeding that on the convex side. With a doping ratio between 1:4 and 1:3 in corannulene, relatively large binding energies indicate stability of $Li_6-C_{20}H_{10}$ and $Li_3-C_{20}H_{10}-Li_2$ complexes. The calculated interaction of H_2 with Li−corannulene complexes is enhanced with respect to that in corannulene. The study of H_2 adsorption on various sites of $Li_2-C_{20}H_{10}$ indicates that lithium atoms are the favorable adsorption sites, with a binding energy of −1.42 kcal/mol compared to −0.92 kcal/mol for the H_2-C interaction.

At the same intermolecular distances, temperature, and pressure, the hydrogen uptake is higher in assemblies of $Li_6-C_{20}H_{10}$ than in those of $Li_3-C_{20}H_{10}-Li_2$. It is shown that separation between molecules is critical to achieve even higher uptakes; for example, at interlayer separations of 10 Å in the $Li_6-C_{20}H_{10}$ complex, the hydrogen uptake reaches 6.5 wt % at 300 K and 215 bar. Such separations may be obtained via substitution of the terminal H atoms in $C_{20}H_{10}$ with bulky terminal groups.

Because our MD results are based on an idealized frozen structure for the adsorbent, further theoretical and experimental studies are needed to prove the adsorbent structure and performance at finite temperatures and pressures.

Acknowledgment. This work is supported by funds from the Air Force Research Laboratory. Supercomputer time provided by the National Energy Research Scientific Computing Center (NERSC), Texas A&M Chemical Engineering departmental computer cluster, and TAMU supercomputer center is gratefully acknowledged.

References and Notes

(1) Forsberg, C. W. *Chem. Eng. Prog.* **2005**, *101*, 20−22.

(2) Schueth, F.; Bogdanovic, B.; Felderhoff, M. *Chem. Commun.* **2004**, *20*, 2249−2258.

(3) Chao, B. S.; Young, R. C.; Myasnikov, V.; Li, Y.; Huang, B.; Gingl, F.; Ferro, P. D.; Sobolev, V.; Ovshinsky, S. R. *Mater. Res. Soc. Symp. Proc.* **2004**, *801*, 27−39.

(4) Ritter, J. A.; Ebner, A. D.; Wang, J.; Zidan, R. *Mater. Today* **2003**, *6*, 18−23.

(5) Bowman, R. C., Jr.; Fultz, B. *MRS Bull.* **2002**, *27*, 688−693.

(6) Hirscher, M.; Becher, M.; Haluska, M.; Dettlaff-Weglikowska, U.; Quintel, A.; Duesberg, G. S.; Choi, Y.; Downes, P.; Hulman, M.; Roth, S.; Stepanek, I.; Bernier, P. *Appl. Phys. A* **2001**, *72*, 129−132.

(7) Ye, Y.; Ahn, C. C.; Witham, C.; Fultz, B.; J. Liu, J.; Rinzler, A. G.; Colbert, D.; Smith, K. A.; Smalley, R. E. *Appl. Phys. Lett.* **1999**, *74*, 2307−2309.

(8) Dillon, A. C.; Jones, K. M.; Bekkedahl, T. A.; Kiang, C. H.; Bethune, D. S.; Heben, M. J. *Nature (London)* **1997**, *386*, 377−379.

(9) Liu, C.; Fan, Y. Y.; Liu, M.; Cong, H. T.; Cheng, H. M.; Dresselhaus, M. S. *Science* **1999**, *286*, 1127−1129.

(10) Ahn, C. C.; Ye, Y.; Ratnakumar, B. V.; Witham, C.; Bowman, R. C., Jr.; Fultz, B. *Appl. Phys. Lett.* **1998**, *73*, 3378−3380.

(11) Browning, D. J.; Gerrard, M. L.; Lakeman, J. B.; Mellor, I. M.; Mortimer, R. J.; Turpin, M. C. *Nano Lett.* **2002**, *2*, 201−205.

(12) Orimo, S.; Majer, G.; Fukunaga, T.; Zuttel, A.; Schlapbach, L.; Fujii, H. *Appl. Phys. Lett.* **1999**, *75*, 3093−3095.

(13) Frankland, S. V.; Brenner, D. W. *Polym. Prepr.* **1999**, *40*, 721−722.

(14) Zhao, Y.; Kim, Y.-H.; Dillon, A. C.; Heben, M. J.; Zhang, S. B. *Phys. Rev. Lett.* **2005**, *94*, 155504.

(15) Trainer, P. D. Treatment of Hydrogen Storage Alloy for Battery Anodes with Organometallic Compound to Provide Alloy with Corrosion Resistance; 1999.

(16) Rao, C. N. R.; Govindaraj, A. *Acc. Chem. Res.* **2002**, *35*, 998−1007.

(17) Rosi, N. L.; Eckert, J.; Eddaoudi, M.; Vodak, D. T.; Kim, J.; O'Keeffe, M.; Yaghi, O. M. *Science* **2003**, *300*, 1127−1130.

(18) Panella, B.; Hirscher, M. *Adv. Mater.* **2005**, *17*, 538541.

(19) Rowsell, J. L. C.; Millward, A. R.; Park, K. S.; Yaghi, O. M. *J. Am. Chem. Soc.* **2004**, *126*, 5666−5667.

(20) Rosi, M.; Sgamellotti, A.; Franceschi, F.; Floriani, C. *Chem.—Eur. J.* **1999**, *5*, 2914−2920.

(21) Meregalli, V.; Parrinello, M. *Appl. Phys. A* **2001**, *72*, 143−146.

(22) Ding, R. G.; Finnerty, J. J.; Zhu, Z. H.; Yan, Z. F.; Lu, G. Q. *Encycl. Nanosci. Nanotechnol.* **2004**, *4*, 13−33.

(23) Schlapbach, L.; Zuttel, A. *Nature (London)* **2001**, *414*, 353−358.

(24) Chen, P.; Wu, X.; Lin, J.; Tan, K. L. *Science* **1999**, *285*, 91−93.

(25) Cao, A.; Zhu, H.; Zhang, X.; Li, X.; Ruan, D.; Xu, C.; Wei, B.; Liang, J.; Wu, D. *Chem. Phys. Lett.* **2001**, *342*, 510−514.

(26) Froudakis, G. E. *Nano Lett.* **2001**, *1*, 531−533.

(27) Zhao, Y. L.; Zhang, R. Q.; Wang, R. S. *Chem. Phys. Lett.* **2004**, *398*, 62−67.

(28) Turker, L.; Gumus, S. *J. Mol. Struct. (THEOCHEM)* **2004**, *684*, 205−209.

(29) Zhu, Z. H.; Lu, G. Q.; Smith, S. C. *Carbon* **2004**, *42*, 2509−2514.

(30) Deng, W.; Xu, X.; Goddard, W. A. *Phys. Rev. Lett.* **2004**, *92*, 166103−166101.

(31) Dubot, P.; Cenedese, P. *Phys. Rev. B* **2001**, *63*, 241402/241401−241404.

(32) Frash, M. V.; Hopkinson, A. C.; Bohme, D. K. *J. Am. Chem. Soc.* **2001**, *123*, 6687−6695.

(33) Scanlon, L. G.; Balbuena, P. B.; Zhang, Y.; Sandi, G.; Back, C. K.; Feld, W. A.; Mack, J.; Rottmayer, M. A.; Riepenhoff, J. L. *J. Phys. Chem. B* **2006**, *110*, 7688−7694.

(34) Janot, R.; Conard, J.; Guerard, D. *Carbon* **2001**, *39*, 1931−1934.

(35) Kang, H. S. *J. Phys. Chem. A* **2005**, *109*, 478−483.

(36) Frisch, M. J.; Trucks, G. W.; Schlegel, H. B.; Scuseria, G. E.; Robb, M. A.; Cheeseman, J. R.; Montgomery, J. A., Jr.; Vreven, T.; Kudin, K. N.; Burant, J. C.; Millam, J. M.; Iyengar, S. S.; Tomasi, J.; Barone, V.; Mennucci, B.; Cossi, M.; Scalmani, G.; Rega, N.; Petersson, G. A.; Nakatsuji, H.; Hada, M.; Ehara, M.; Toyota, K.; Fukuda, R.; Hasegawa, J.; Ishida, M.; Nakajima, T.; Honda, Y.; Kitao, O.; Nakai, H.; Klene, M.; Li, X.; Knox, J. E.; Hratchian, H. P.; Cross, J. B.; Bakken, V.; Adamo, C.; Jaramillo, J.; Gomperts, R.; Stratmann, R. E.; Yazyev, O.; Austin, A. J.; Cammi, R.; Pomelli, C.; Ochterski, J. W.; Ayala, P. Y.; Morokuma, K.; Voth, G. A.; Salvador, P.; Dannenberg, J. J.; Zakrzewski, V. G.; Dapprich, S.; Daniels, A. D.; Strain, M. C.; Farkas, O.; Malick, D. K.; Rabuck, A. D.; Raghavachari, K.; Foresman, J. B.; Ortiz, J. V.; Cui, Q.; Baboul, A. G.; Clifford, S.; Cioslowski, J.; Stefanov, B. B.; Liu, G.; Liashenko, A.; Piskorz, P.; Komaromi, I.; Martin, R. L.; Fox, D. J.; Keith, T.; Al-Laham, M. A.; Peng, C. Y.; Nanayakkara, A.; Challacombe, M.; Gill, P. M. W.; Johnson, B.; Chen, W.; Wong, M. W.; Gonzalez, C.; Pople, J. A. *Gaussian 03*, revision C.02; Gaussian, Inc.: Wallingford, CT, 2004.

(37) Martin, J. M. L.; Alsenoy, C. V. *J. Phys. Chem.* **1996**, *100*, 6973−6983.

(38) Baldridge, K. K.; Siegel, J. S. *Theor. Chem. Acc.* **1997**, *97*, 67−71.

(39) Jursic, B. S. *THEOCHEM* **1999**, *487*, 193−203.

(40) Rappe, A. K.; Casewit, C. J.; Colwell, K. S.; Goddard, W. A.; Skiff, W. M. *J. Am. Chem. Soc.* **1992**, *114*, 10024−10035.

(41) Gready, J. E.; Bacskay, G. B.; Hush, N. S. *Chem. Phys.* **1977**, *22*, 141−150.

(42) Smith, W.; Forester, T. R. *DL_POLY*; Daresbury Laboratory: Daresbury, U.K., 1996.

(43) Lovas, F. J.; McMahon, R. J.; Grabow, J.-U.; Schnell, M.; Mack, J.; Scott, L. T.; Kuczkowski, R. L. *J. Am. Chem. Soc.* **2005**, *127*, 4345−4349.

(44) Guay, P.; Stanfield, B. L.; Rochefort, A. *Carbon* **2004**, *42*, 2187−2193.

(45) Darkrim, F.; Levesque, D. *J. Phys. Chem. B* **2000**, *104*, 6773−6776.

(46) Simonyan, V. V.; Johnson, J. K. *J. Alloys Compd.* **2002**, *330−332*, 659−665.

(47) Zhang, Y.; Scanlon, L. G.; Balbuena, P. B. Hydrogen Adsorption in Corannulene-Based Materials. In *Nanomaterials: Design and Simulation*; Balbuena, P. B., Seminario, J. M., Eds.; Elsevier Science Publishers: Amsterdam, 2006; Vol. 18, pp 127−166.